Journal of Marine Science and Technology

Volume 24 | Issue 3 Article 32

HIGH-RESOLUTION SURFACE CIRCULATION OF THE BAY OF BENGAL DERIVED FROM SATELLITE OBSERVATION DATA

Mridula Kuttyattu Rayaroth
Department of Geoinformation, Faculty of Geoinformation and Real Estate, Universiti Teknologi Malaysia, Johor, Malaysia

Benny Neettumkara
Department of Coastal and Offshore Engineering, School of Ocean Engineering and Underwater Technology, Kerala University of Fisheries and Ocean Studies, Kochi, India., bennynpeter@gmail.com

Mohd Razali Mahmud
Department of Geoinformation, Faculty of Geoinformation and Real Estate, Universiti Teknologi Malaysia, Johor, Malaysia

Recommended Citation

Rayaroth, Mridula Kuttyattu; Neettumkara, Benny; and Mahmud, Mohd Razali (2016) "HIGH-RESOLUTION SURFACE CIRCULATION OF THE BAY OF BENGAL DERIVED FROM SATELLITE OBSERVATION DATA," *Journal of Marine Science and Technology*: Vol. 24: Iss. 3, Article 32.
DOI: 10.6119/JMST-015-1215-2
Available at: https://jmstt.ntou.edu.tw/journal/vol24/iss3/32

HIGH-RESOLUTION SURFACE CIRCULATION OF THE BAY OF BENGAL DERIVED FROM SATELLITE OBSERVATION DATA

Acknowledgements

The first author acknowledges financial support for the work from Fundamental Research Grant Scheme (FRGS) research grant Vote no. RJ1310000.7827.4F586, Ministry of Higher Education (MOHE). We used the altimeter data set produced by the Collect Localisation Satellites, the drifter data produced by the Atlantic Oceanographic and Meteorological Laboratory of the National Oceanic and Atmospheric Administration, and the wind data set produced and provided by the French Processing and Archiving Facility (CERSAT) at the French Research Institute for Exploration of the Sea. We used the Ocean Data View by R. Schlitzer (http://odv.awi.de, 2013), for preparing graphics. We appreciate the detailed and helpful comments of the anonymous reviewers of this manuscript

Journal of Marine Science and Technology, Vol. 24, No. 3, pp. 656-668 (2016)
DOI: 10.6119/JMST-015-1215-2

HIGH-RESOLUTION SURFACE CIRCULATION OF THE BAY OF BENGAL DERIVED FROM SATELLITE OBSERVATION DATA

Mridula Kuttyattu Rayaroth[1], Benny Neettumkara Peter[2], and Mohd Razali Mahmud[1]

Key words: satellite altimetry, surface drifter, Bay of Bengal, surface circulation, Indian Ocean Dipole.

ABSTRACT

High-resolution surface circulation and its variability of the Bay of Bengal are derived by combining surface drifter and satellite observation data. The satellite altimetry data, satellite-tracked surface drifter data and ocean surface winds from satellite scatterometers during 1993-2012 are used. The estimated velocities show good agreement with in-situ acoustic Doppler current profiler observations. The estimated velocity components are significantly correlated with monthly mean velocity components from Research Moored Array for African-Asian-Australian Monsoon Analysis and Prediction buoy data. The mean circulation exhibits the strong western boundary current, zonal currents and weak eastern boundary flow. Large spatial and temporal variations are found in the western boundary current and intense mesoscale eddy activity in the western Bay of Bengal. Significant changes in surface circulation during positive and negative Indian Ocean Dipole (IOD) events are evident. During positive IOD, the eastward equatorial jet is reversed and the western boundary current is much weakened. Meanwhile, the western boundary current is the prominent flow during negative IOD events. High eddy kinetic energy is found during strong IOD events.

I. INTRODUCTION

The Bay of Bengal (BoB), the northeastern arm of the Indian Ocean, is a unique ocean with interrelated oceanographic, biological and sedimentary processes driven by monsoon winds. The semi-enclosed nature and the proximity to the equator make the BoB different from other oceans (Fig. 1). Systematic information on the BoB was first obtained from the studies (Duing, 1970; Wyrtki, 1971, 1973) conducted during the International Indian Ocean Expedition in 1960-1965.

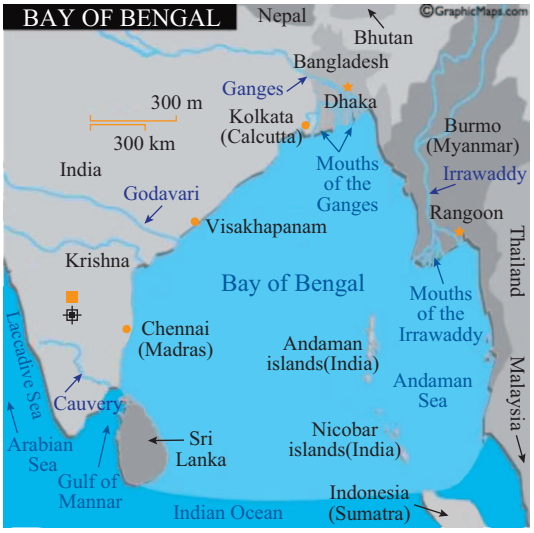

Fig. 1. Geographic location of Bay of Bengal (image taken from https://mygoldenbengal.wordpress.com).

A unique feature of the bay is the extreme variability of its physical properties. Sea surface temperature (SST) in the BoB has significant influence on the climate and monsoon precipitation over the surrounding land masses (Li et al., 2001; Shenoi et al., 2002; Shankar et al., 2007; Jiang and Li, 2011). The SST over BoB is much warmer than that over the Arabian Sea (Shenoi et al., 2002). Temperature in the offshore areas, however, is warm and markedly uniform in all seasons, decreasing somewhat towards the north.

Salinity distribution of BoB is highly heterogeneous with extremely fresh surface water in the northern part of the basin and saltier water at subsurface as well as towards the south. Several studies (e.g., Murty et al., 1992, 1996; Shetye et al.,

Paper submitted 05/11/15; revised 10/07/15; accepted 12/30/15. *Author for correspondence: Benny Neettumkara Peter (e-mail: bennynpeter@gmail.com).*
[1] *Department of Geoinformation, Faculty of Geoinformation and Real Estate, Universiti Teknologi Malaysia, Johor, Malaysia.*
[2] *Department of Coastal and Offshore Engineering, School of Ocean Engineering and Underwater Technology, Kerala University of Fisheries and Ocean Studies, Kochi, India.*

1996; Pant et al., 2015) investigated the variability of sea surface salinity (SSS) in the BoB. The density distribution in the BoB shows large salinity-induced variations. For example, at the head of the BoB, density is relatively low and varies extensively throughout the year. Conversely, it is relatively high in the southern portion of the area where salinity is high.

The BoB surface circulation comprises of the zonal North Equatorial Current (NEC; also called the Winter Monsoon Current), the Southwest Monsoon Current (also called the Summer Monsoon Current), coastal currents, gyres, eddies, fronts, etc., and is influenced by low frequency wave activity (Chelton et al., 2007; Rao et al., 2009). Among these, the monsoon currents are the most prominent large scale currents. In summer, the Southwest Monsoon Current flows eastward as a broad continuous band from the western Arabian Sea to the BoB. In winter, the NEC flows westward between 8°N and the equator (Pickard and Emery, 1982) from the eastern boundary of the BoB to the western Arabian Sea, transporting low salinity water from the BoB to the Arabian Sea. The transition periods between monsoons (April-May and October-November) are marked with intense eastward equatorial jets known as Wyrtki jets (Wyrtki, 1973) and this Wyrtki jets significantly influence the circulation of the BoB. Concentrating the entire eastward flow in a 600 km wide band along the equator, the jet reaches its peak in November with speed of 1.0-1.3 m/s and disappears in early January, when the annual cycle is restarted (Tomzeck and Godfrey, 1994).

The NEC is comparatively weak in the annual mean circulation (Benny and Mizuno, 2000). The Summer Monsoon Current intensifies and shifts westwards as the summer monsoon progresses (Vinayachandran et al., 1999a). This westward shift with time is also identified in the surface geostrophic flow estimated from the TOPEX/Poseidon altimeter (Eigenheer and Quadfasel, 2000). The western boundary current, called the East Indian Coastal Current (EICC), is about 900 km in length (Reddy et al., 1995), usually lying close to the east coast of India, but occasionally shifting offshore (Shetye et al., 1993) with an average speed of 0.3-0.6 m/s. Hydrographic studies (Shetye et al., 1993; Stramma et al., 1996; Sanilkumar et al., 1997) and numerical studies (McCreary et al., 1996; Shanker et al., 1996) further described the western boundary current and its driving mechanisms.

The BoB exhibits seasonally-reversing monsoon circulation along with depressions, severe cyclonic storms and comparatively low saline surface waters due to the large amount of river run-off from the Indian subcontinent. Strong surface circulations embedded with counter-clockwise gyres have been noticed (Potemra et al., 1991). The steadiness and strength of the gyres and currents seem to depend on the development and latitudinal shift of the NEC and Summer Monsoon Current (Varkey et al., 1996).

The equatorial Kelvin wave propagating eastward splits into two coastal Kelvin waves at the eastern boundary of the Indian Ocean; the northward signal propagates along the rim of the BoB and Andaman Sea (Potemra et al., 1991), leading to remotely-driven coastal currents, which may radiate long Rossby waves. Those Rossby waves propagate westward and influence currents in the interior and western boundary region of the BoB (Shetye et al., 1993; McCreary et al., 1996).

The Indian Ocean Dipole (IOD) has been identified (Saji et al., 1999; Webster et al., 1999) as the largest and unique inter-annual variability in the Indian Ocean. Besides SST anomaly variation, IOD is associated with other ocean-atmosphere processes and temperature anomalies are also found in sub-surface levels of the ocean (Vinayachandran et al., 2002; Horii et al., 2008). Moreover, the zonal wind anomalies during IOD events weaken or reverse the equatorial jet (Vinaychandran et al., 1999b). Many studies (Yamagata et al., 2002; Annamailai et al., 2003; Halkides et al., 2006; Meyers et al., 2007; Vinayachandran et al., 2007) have reported the characteristics of different IOD events. The ocean-atmosphere coupling during IOD involves atmospheric convection, winds, SST and upper ocean dynamics (Vinayachandran et al., 2009; Aparna et al., 2012).

However, as systematic observational networks are not available for BoB, the details on scales of motion and its variability have not been known due to the scarcity of in-situ observations. Hence, the present study envisions achieving two important goals,by employing satellite observational data. First, it derives a new high-resolution (1/3° latitude × 1/3° longitude) mean surface velocity field, by combining satellite altimeter and satellite-tracked drifter observations from 1993 to 2012, and validates the velocity field using available in-situ observations. Secondly, it confirms the seasonal and inter-annual variability of surface circulation and IOD/El Niño effects on flow pattern, through examining time series of surface velocity field derived from combining the above-mentioned mean field and satellite altimetry data. The rest of the paper is organized as follows. Section 2 describes the data used and the methodology followed. Section 3 presents the results from the analyses and discusses the mean, seasonal and inter-annual surface circulations. Finally, the derived conclusions are summed up in section 4.

II. DATA AND ANALYSIS

The surface drifter data used in this study comes from the Global Drifter Program (Surface Velocity Program, http://www.aoml.noaa.gov/). Positions of freely drifting buoys with drogues at 15 m depth were located using the ARGOS satellite system. Data used were quality controlled and optimally interpolated to uniform six-hour interval trajectories using the drifter's position data. This data set has been compiled and maintained by the Drifter Data Center at the Atlantic Oceanographic and Meteorological Laboratory of the National Oceanic and Atmospheric Administration, USA. The density of drifter data available in the period 1993-2012 is given in Fig. 2.

The satellite altimetry data used in this study are Maps of Sea Level Anomaly produced by the Collect Localization Satellites, France. The sea level anomalies were obtained by

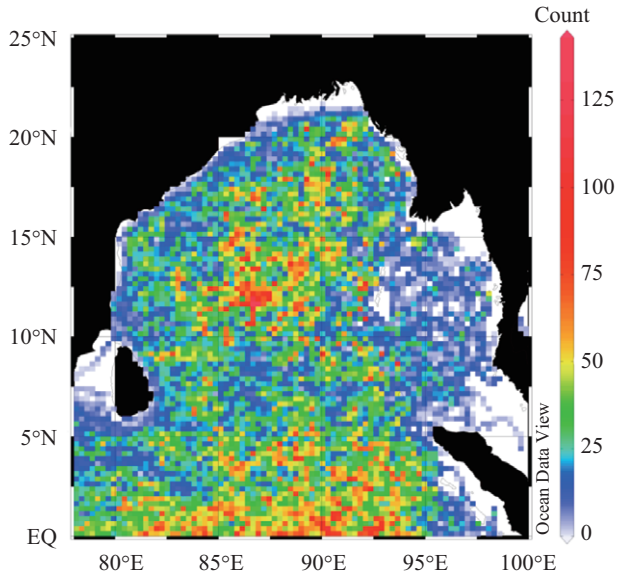

Fig. 2. Number of drifter data in each box of 1/3° latitude × 1/3° longitude in the BoB during 1993-2012.

merging Jason/TOPEX/Poseidon and ERS/Envisat altimetry data using optimal interpolation (AVISO1997, http://www.aviso.Oceanobs.com). Maps have been produced weekly since September 1992 with a resolution of 1/3° latitude and 1/3° longitude. The weekly mean ocean surface wind fields derived from the scatterometers on board ERS-1/2, QuikSCAT and ASCAT, generated by "Centre ERS d'Archivage et de Traitement" (CERSAT), France (http://cersat.ifremer.fr/) are used to estimate the wind-driven Ekman velocity.

In this study, the surface drifter and altimetry data are combined to estimate the mean surface velocity. At a location **x** and time t, the instantaneous geostrophic velocity **Vg (x,** t**)** can be written as,

$$\mathbf{Vg}\,(\mathbf{x}, t) = \mathbf{Vmg}\,(\mathbf{x}) + \mathbf{Vg'}\,(\mathbf{x}, t) \quad (1)$$

Where, **Vmg (x)** is the mean geostrophic velocity over some observational period and **Vg' (x,** t**)** is the geostrophic velocity anomaly from the temporal mean. Therefore,

$$\mathbf{Vmg}\,(\mathbf{x}) = \mathbf{Vg}\,(\mathbf{x}, t) - \mathbf{Vg'}\,(\mathbf{x}, t) \quad (2)$$

The instantaneous geostrophic velocity can be obtained from the drifter observations. The geostrophic velocity anomaly can be obtained from the altimetry sea level anomalies. Hence, the mean velocity can be calculated by subtracting the altimeter-derived geostrophic velocity anomaly from the drifter-derived instantaneous geostrophic velocity measured at the same time and location (Uchida and Imawaki, 2003; Benny et al., 2014). This method estimates almost unbiased Eulerian mean velocities which are free from the sampling tendency of the drifters. The average of the calculated mean velocities in each grid gives a more accurate estimate by reducing the estimation error.

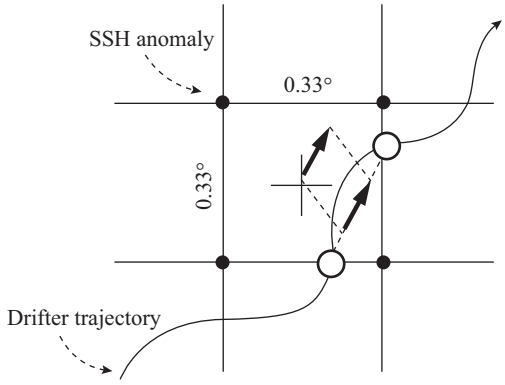

Fig. 3. Schematic diagram showing the method to calculate a velocity from a low-pass-filtered drifter trajectory (adapted from Uchida and Imawaki (2003)). The velocity for a 1/3° latitude × 1/3° longitude box defined by grid points of the altimeter data set is calculated from two positions (open circles) and times where and when a drifter comes in and goes out the box.

Before the calculation, the drifter trajectories are low-pass filtered by a 60 hour running mean to remove the high frequency fluctuations. Then the drifter data has been gridded into 1/3° latitude × 1/3° longitude boxes which are used for the above-mentioned Maps of Sea Level Anomaly. The surface velocity has been estimated from the drifter position data in each grid as shown in Fig. 3. The wind-produced slip is corrected by employing the Niiler and Paduan (1995) method. An additional correction is made for drifters which had lost their drogues during their traverse, using the empirical relation given by Pazan and Niiler (2001). The Ekman velocity is estimated by using the ocean surface winds from scatterometer observations and employing the Ralph and Niiler (1999) model as,

$$\mathbf{V_E} = A.\,|f|^{-1/2}.\,\mathbf{W.\,exp\,(i.\,\theta)} \quad (3)$$

Where, $\mathbf{V_E} = U_E + \mathbf{i}.V_E$, is the Ekman velocity at 15 m depth, $A = 7 \times 10^{-7}\ s^{-1/2}$, f is the Coriolis parameter, and W is the wind speed. The term **exp (i .θ)** (**θ** = ± 54**)** represents the rotation of the Ekman velocity to the right-hand-side of the wind vector in the northern hemisphere. The instantaneous geostrophic velocity **Vg (x,** t**)** is estimated by subtracting the Ekman velocity from the drifter velocity.

The zonal and meridional components (u, v) of geostrophic velocity anomaly **Vg' (x,** t**)** are computed from altimetry sea level anomaly data using the conventional geostrophic relation.

$$u = -\,g/f\,(\partial h/\partial y) \quad (4)$$

$$v = g/f\,(\partial h/\partial x) \quad (5)$$

Where g is the acceleration due to gravity, h is the sea surface height anomaly, x is the distance in zonal direction; y is the distance in meridional direction. Since the geostrophic approximation is not valid near the equator, the estimation of velocity anomaly is limited down to 1°N.

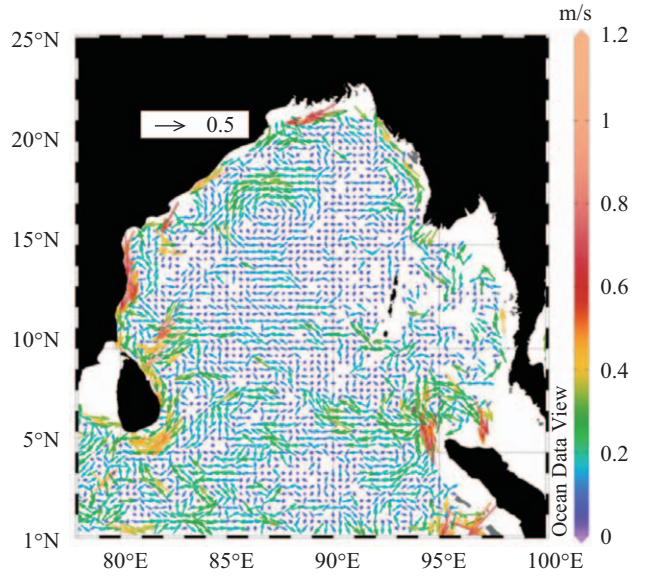

Fig. 4a. Mean geostrophic velocity field (Vmg (x)) derived by combining satellite altimetry (Fig. 4b) and surface drifter observations (Fig. 4c); namely, Vmg (x) = Vg (x, t) - Vg' (x, t).

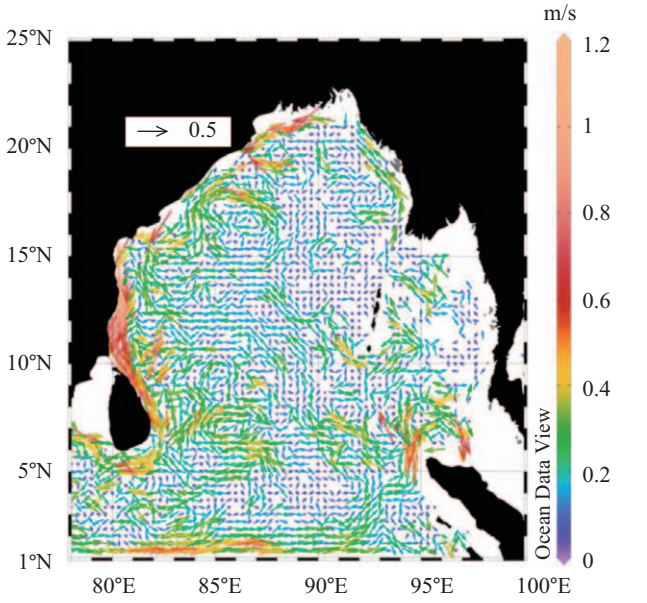

Fig. 4c. Map of simple average of instantaneous geostrophic velocities estimated from surface drifter data, Vg (x, t).

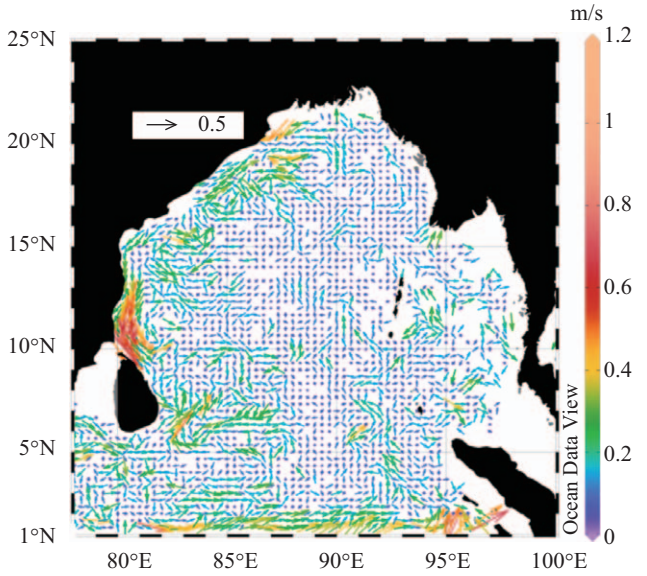

Fig. 4b. Map of average of altimeter-derived geostrophic velocity anomalies at the time of drifter measurements, Vg' (x, t).

In this study, we estimate mean velocities only at locations where five or more drifter observations are available. The time series of geostrophic velocity is obtained by adding the above-mentioned mean geostrophic velocity to the geostrophic velocity anomaly derived from satellite altimetry data.

III. RESULTS AND DISCUSSIONS

The Eulerian mean velocity field obtained by combining the satellite altimetry and drifter data reveals the details of surface flow pattern of BoB (Fig. 4a). The average of altimeter-derived velocity anomalies at the time of drifter measurements (Fig. 4b) serves as correction to the simple average of the drifter-derived velocities (Fig. 4c).

Although the large scale flow pattern of the mean geostrophic velocity field is not much different from the simple average of drifter-derived velocity field, the above-mentioned correction by the altimeter-derived velocity anomaly shows significant differences along the peripherals and variations found especially in the western part and near the equator. Maximum anomaly of about 0.7 m/s is found along the east coast of India, whereas the eastern and northern BoB show comparatively weak (< 0.3 m/s) anomaly. Anomaly field is also prominent in the zonal eastward flow near the equator, where the variations up to 0.5 m/s are found. The seasonal reversal of flow in the near equatorial region and the presence of monsoon transitional equatorial Jet flow causes large anomaly field near the equator.

1. Comparison with In-Situ Observations

The velocity field estimated by combining satellite observational data is compared with in-situ observational data, including available Research Moored Array for African-Asian-Australian Monsoon Analysis and Prediction (RAMA) buoy data, acoustic Doppler current profiler (ADCP) data and salinity section. The RAMA buoy data is available at three locations of 8°N, 12°N and 15°N along 90°E. The monthly mean velocity components obtained from the RAMA buoy moored at 10 m are compared with the monthly mean components estimated in the present study (Fig. 5a).

Significant correlation is obtained between the observed

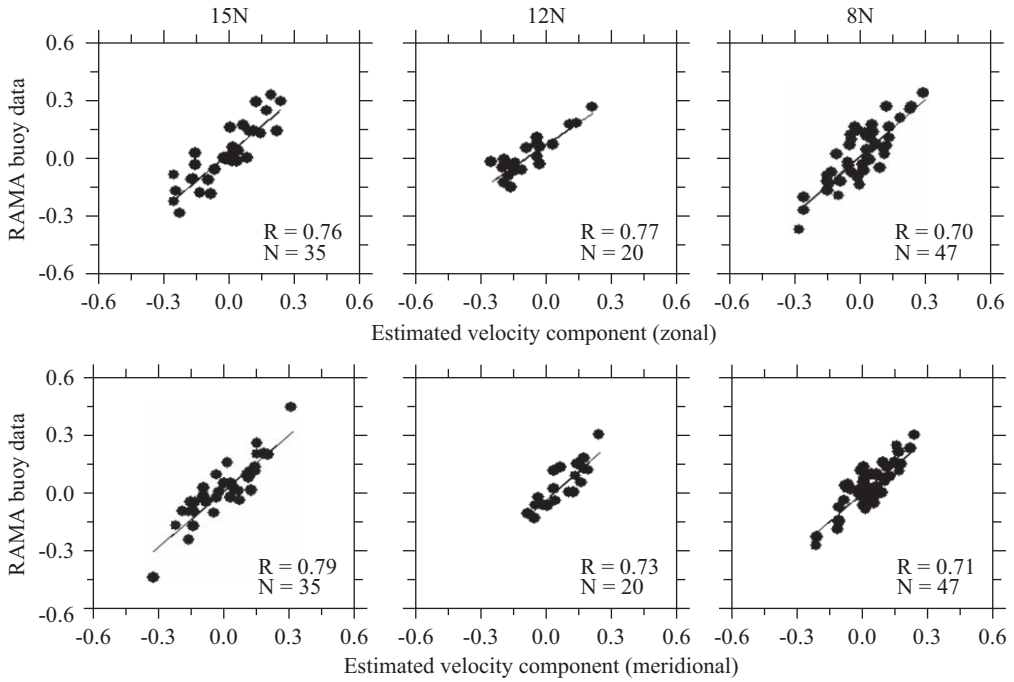

Fig. 5a. Comparison of estimated geostrophic velocity components (abscissa) with RAMA buoy data (ordinate) obtained at 15°N (left panel), 12°N (middle) and 8°N (right) at 90°E. The upper panel shows the zonal component and lower panel, the meridional component. The unit is m/sec.

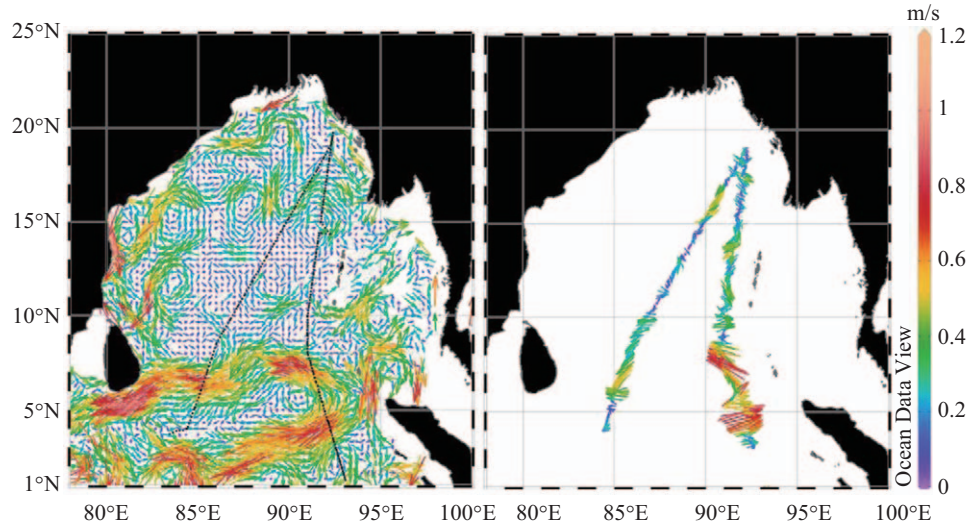

Fig. 5b. Comparison of estimated geostrophic velocity field with in-situ ADCP observations during February 1995. The left panel shows estimated monthly mean velocity field and right panel shows ADCP observations.

and estimated velocity components at all the three locations. The correlation coefficients for both the zonal and meridional components are above 0.70 and highest correlation is found at 15°N site. Number of observations is less at 12°N and the comparison for 12°N is less satisfactory than 8°N and 15°N.

In order to validate our estimated velocity field, we make visual comparison with in-situ ADCP observations obtained in February-March 1995 during the World Ocean Circulation Experiment (WOCE). The estimated monthly mean geostrophic velocity field of February 1995 and the ADCP velocity data at 30 m depth are shown in Fig. 5b. The ADCP observations were made along two meridional tracks in the central part between 85°E and 95°E, from the equator up to around 19°N. The overall current pattern and the speed range of ADCP observations are in good agreement with the estimated velocity field. On the eastern track, the maximum eastward current with speed of 0.7 m/s is observed at around 5°N in the ADCP observations as well as in the estimated filed. Also, strong

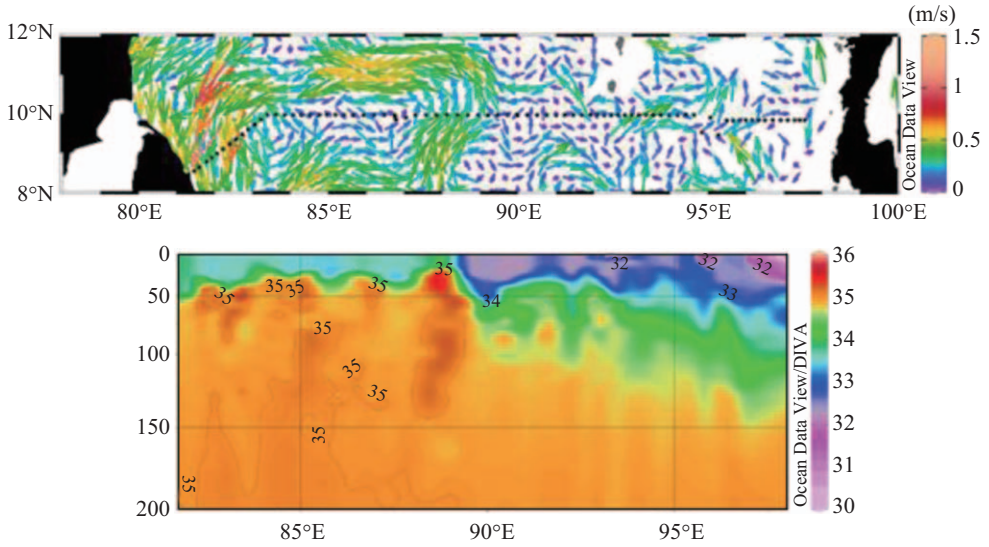

Fig. 5c. Comparison of estimated geostrophic velocity field with salinity distribution in October 1995. The upper panel shows estimated monthly velocity field and the WOCE IO 1E hydrographic stations marked as black dots. The lower panel shows vertical section of salinity along the WOCE IO 1E.

westward return flow around 7°N is clearly visible in both maps. Fig. 5c. Comparison of estimated geostrophic velocity field with salinity distribution in October 1995. The upper panel shows estimated monthly velocity field and the WOCE IO 1E hydrographic stations marked as black dots. The lower panel shows vertical section of salinity along the WOCE IO 1E. Between 14°N and 15°N, south-westward flow is identical in both estimated and observed fields. Similarly, on the western track, the ADCP observation shows southeastward flow between 15°N and 16°N, and strong south-westward flow between 5°N and 7°N, which are well illustrated in the estimated filed with similar speeds.

Also compared is the salinity distribution along a zonal section on approximately 10°N covered in October 1995 during the WOCE, which extends approximately from 81°E to 97°E. The vertical section of salinity down to 200 m depth is prepared and compared with the estimated monthly mean geostrophic velocity field in October 1995 (Fig. 5c).

The salinity distribution shows a frontal structure at around 89°E, where the low salinity water from the east and high salinity water from the west face to each other and about 1 psu salinity difference is found in the surface layer. The estimated circulation pattern during October 1995 clearly explains the structure that the strong northward flow observed between 87°E and 89°E carries the high salinity water from the southwest to this region. The boundary of the northward flow coincides with the western extent of the low salinity water from the east. Further, the northward flow takes a cyclonic turn southward and again crosses the 10°N at the western end between 82°E and 83°E, where also high salinity is visible in the section.

2. Mean Velocity Field

Southward flowing EICC on the western boundary of BoB is the prominent current in the mean field (Fig. 4a) and is visible from the head of the BoB as a narrow and strong southward flow along the east coast of India down to south of Sri Lanka. The flow is intense between 12°N and 16°N, where the speed reaches 1 m/s and a confluence of current is observed at around 10°N, where zonal westward flows merge with the southward current. An anticyclonic eddy centered at 16.6°N, 87.0°E and a weak cyclonic eddy adjacent to it in the north are the other prominent features in the western part.

In the southern BoB, a weak broad westward flow of NEC is visible with speed ranging between 0.25 and 0.5 m/s. The core of the flow is located around 6°N and is wide and strong in the eastern part; the flow splits into two branches at 89°E. Eastward flow prevails between 1°N and 2°N with a speed of 0.5 m/s and the area between the westward NEC and eastward equatorial flow is embedded with weak eddies.

The eastern BoB that includes the Andaman Sea and Malacca Strait shows no organised circulation pattern in the mean field. However, traces of northward flow are visible along the eastern boundary. A strong anticyclonic eddy circulation is visible at the entrance of Malacca Strait north of Sumatra Island. In the northern part of the BoB, northward flow prevails along the eastern side with an average speed of 0.4 m/s and feeds the EICC. The central BoB exhibits dull circulation with speeds of less than 0.2 m/s.

3. Seasonal Circulation

The monthly mean geostrophic velocities in January, April, July and October averaged over twenty years (1993-2012) are presented (Fig. 6) to determine the seasonal circulation characteristics of the BoB.

The westward flowing NEC is present most of the months with varying current width and speed. The fully developed

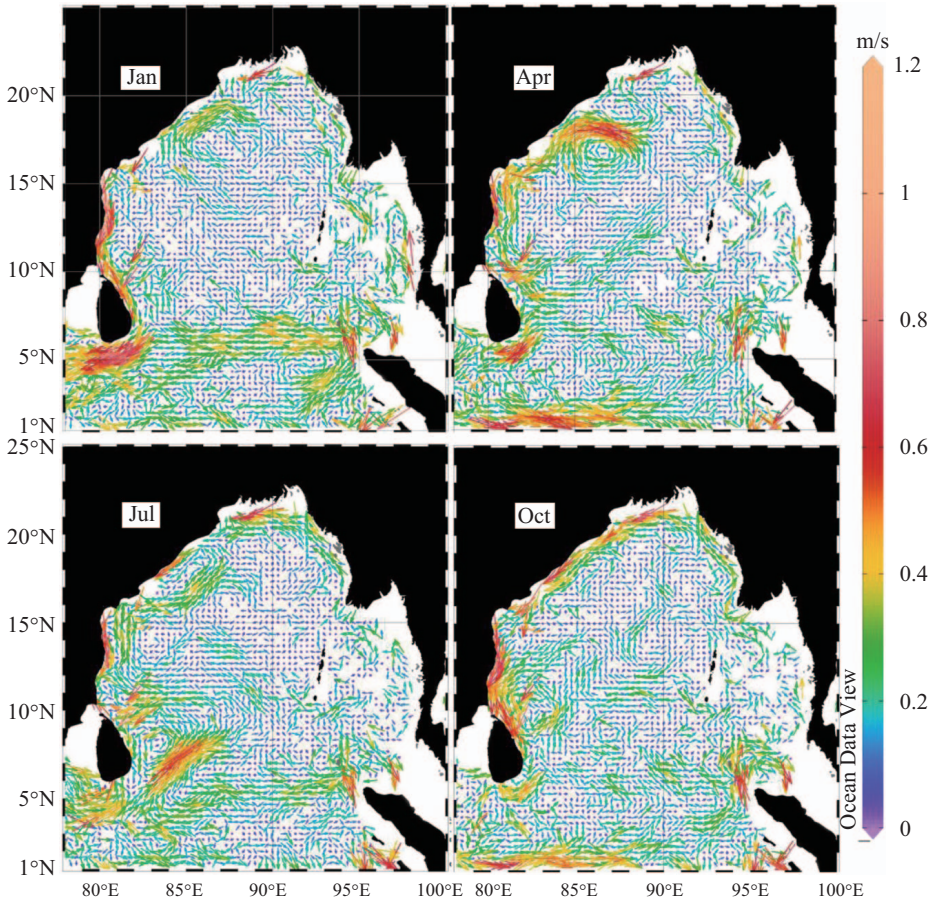

Fig. 6. Monthly mean geostrophic velocity fields in January, April, July and October, averaged over twenty years (1993-2012).

pattern of NEC is visible in January between 5°N and 8°N with speed of about 0.4 m/s in the east and broadens towards the west. When it reaches around 85°E, it slightly bifurcates. The major part of the NEC merges with the southward flowing EICC, flows around southern coast of Sri Lanka and proceeds as a mighty flow between 2°N and 7°N with speeds of up to 0.8 m/s towards Arabian Sea. A minor part of the westward flow takes a cyclonic turn and joins the eastward flow between 1°N and 2°N. As the northeasterly trade wind weakens by March, the NEC in April is too weak and the major part of this weak west-ward flow takes a cyclonic turn west of Sri Lanka and supports the eastward equatorial jet near the equator. In July, the NEC is strengthened and flows between 4°N and 6°N towards the west up to 84°E, where it merges with the Summer Monsoon Current. In October, the NEC is not prominent but some scattered westward flow is visible between 6°N and 7°N.

In January, the strong southward flow of EICC along the east coast of India is visible from 17°N with higher speeds of up to 1 m/s between 12°N and 15°N. In April, the EICC has been reversed and a northward flow occupies most part off the east coast of India. However, traces of southward flow are visible very near to the coast. In July, the southward flow close to the east coast of India is slightly strengthened, but northward flow still dominates away from the coast. The south-ward flow of EICC is well developed in October even from the head of the BoB along the east coast of India and intense flow exists between 8°N and 15°N. The EICC is the most varying current system in the BoB; remotely-forced, coastally-trapped waves and Rossby waves crossing the interior of the BoB are the major contributors to EICC variability (Schott and McCreary, 2001).

The seasonal displacement of western-boundary confluence (Eigenheer and Quadfasel, 2000) is identified in the velocity fields. During January, at the peak of the winter monsoon, the southward EICC decreases in strength and even reverses its direction north of 15°N. The confluence is at 16°N in January and at 10°N in April. The cyclonic and anticyclonic eddies observed in July are consistent with the observations of Paul et al. (2009). A similar flow pattern found along the western boundary and a cyclonic eddy has been reported from hydrographic data (Sanilkumar et al., 1997) and GEOSAT altimetry data (Babu et al., 2003). In late September, the EICC begins to flow southwards, and by November currents flow southwards everywhere along the east coast of India and Sri Lanka (Schott and McCreary, 2001).

The broad eastward flow of Summer Monsoon Current is visible in July between 1°N and 8°N with a speed of 0.5 m/s up to 87°E. As the Summer Monsoon Current advances eastward, it merges with the westward flow at around 84°E and 5°N.

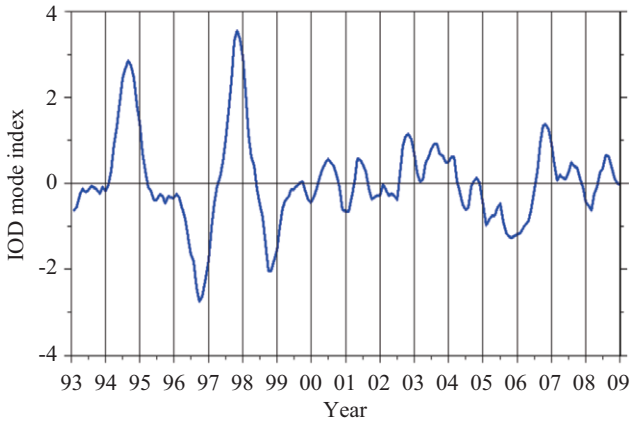

Fig. 7a. Time series of IOD mode index, adapted from "Indian Ocean Dipole" Website (http://www.jamstec.go.jp/).

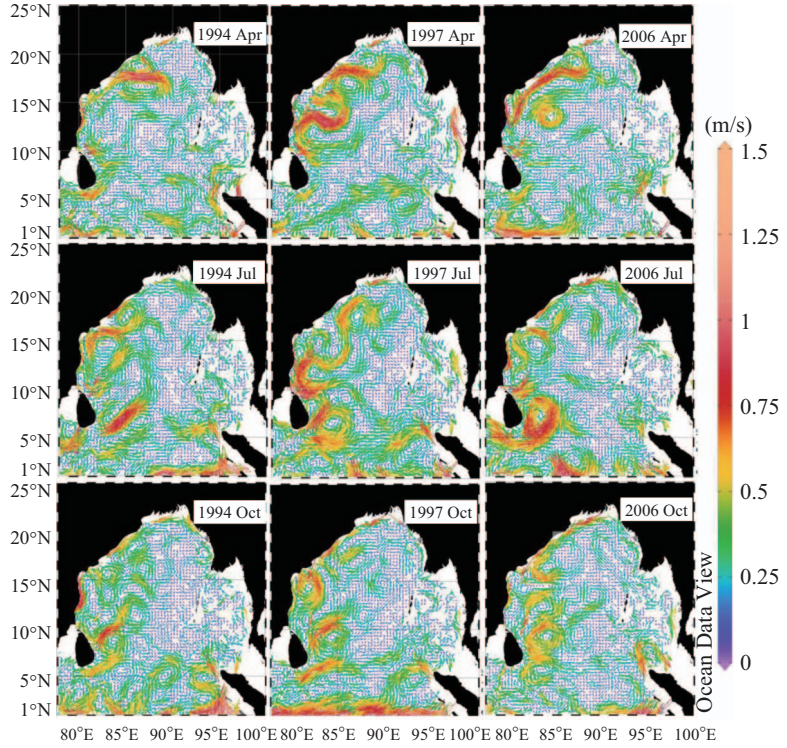

Fig. 7b. Monthly mean geostrophic velocity fields in April (upper panel), July (middle) and October (lower), in 1994 (left), 1997 (middle) and 2006 (right).

Interestingly, a major part of the Summer Monsoon Current is formed as a strong cyclonic eddy (Schott and McCreary, 2001) on the eastern side of Sri Lanka and no significant component of Summer Monsoon Current towards the east.

The flow is quite weak in the eastern side and Andaman Sea compared to that in the western side. In January, a weak cyclonic eddy circulation prevails in the eastern part of Andaman Sea with speeds of up to 0.5 m/s. A strong anticyclonic eddy exists at the entrance of Malacca Strait north of Sumatra Island. Northward flow is visible along the eastern boundary of the BoB between 16°N and 21°N in April and the cyclonic eddy observed in January is weakened and southward flow prevails in the western part of Andaman Sea. In July, the northward flow along the northern part of eastern boundary of the BoB is strengthened and turns westward with speeds of up to 0.8 m/s around the head of the BoB. Weak cyclonic circulation exists in the Andaman Sea and southeastward flow with speeds of up to 0.6 m/s is visible towards Malacca Strait. Northward flow prevails along the whole eastern boundary of the BoB during October.

The presence of eastward-flowing equatorial jet (Wyrtki, 1973) which extends up to 2.5°N with speeds of about 0.7 m/s is identified in both April and October. In both the spring and fall, the jet extends up to 92°E and branches southward and northward between 90°E and 92°E. Away from the equator (north of 3°N), the current speed falls off to less than 0.2 m/s.

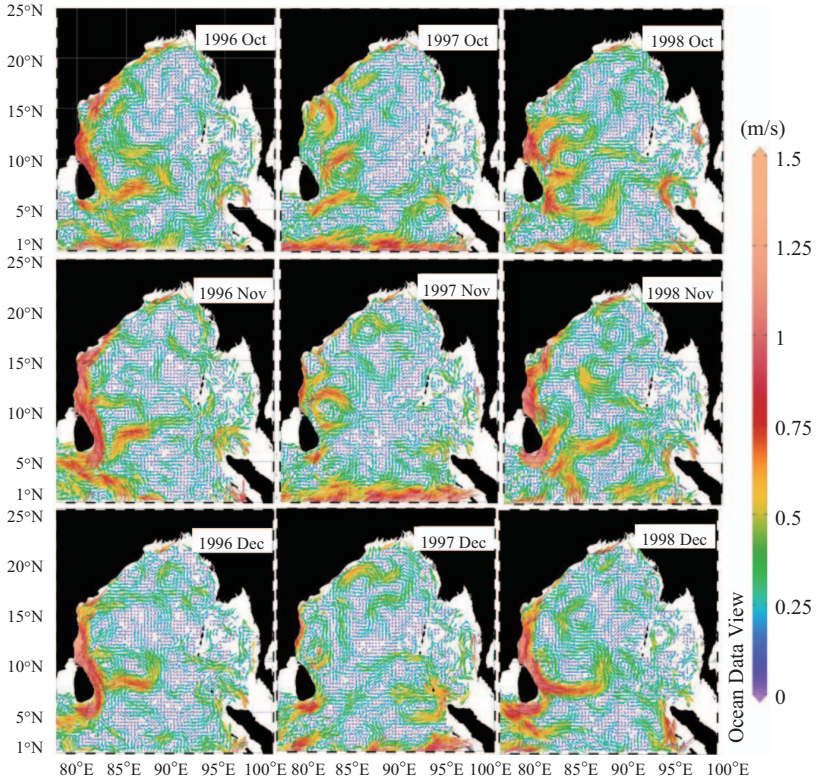

Fig. 7c. Monthly mean geostrophic velocity fields in October (upper panel), November (middle) and December (lower), in 1996 (left), 1997 (middle) and 1998 (right).

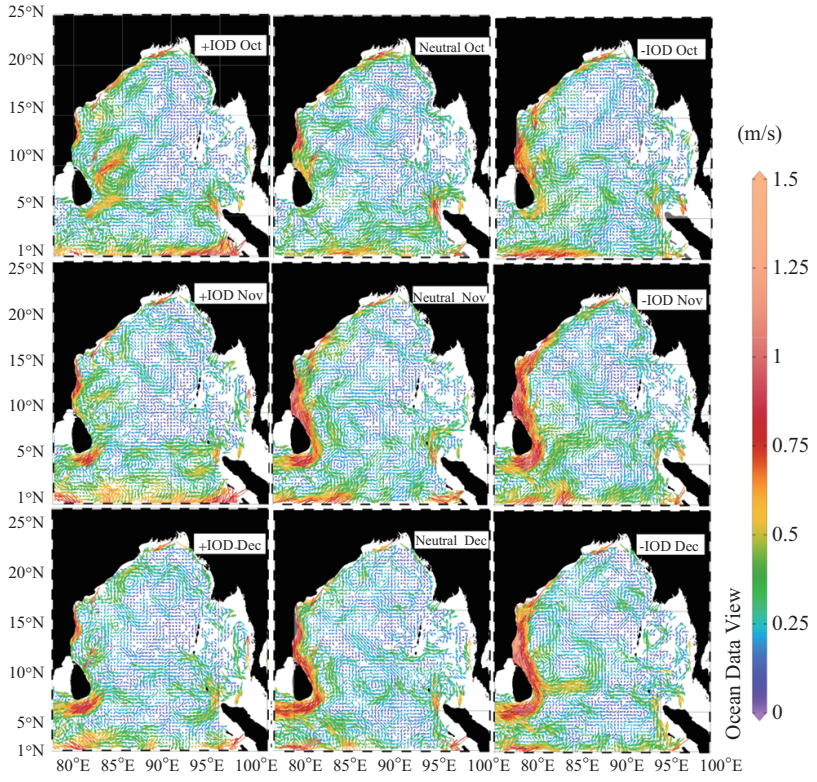

Fig. 7d. Composite maps of geostrophic velocity fields in October (upper panel), November (middle), and December (lower) for positive (left), neutral (middle) and negative (right) IOD years.

In addition to strong currents, BoB exhibits strong mesoscale eddy activity. In January, an anticyclonic eddy centered at 18°N, 87°E in the western side and another one near the entrance of Malacca Strait are visible. The former anticyclonic eddy is further strengthened in April and another weak cyclonic eddy develops adjacent to it in the north. A cyclonic eddy also appears between Sri Lanka and equator in the south. In July, the anticyclonic eddy has disappeared and instead a cyclonic eddy has developed between 15°N and 20°N near the east coast of India. Another strong cyclonic eddy has developed by the Summer Monsoon Current off the northeast of Sri Lanka. The cyclonic eddies have weakened by October in the western part, but the anticyclonic eddy has strengthened at the entrance of Malacca Strait off the north of Sumatra.

4. Surface circulation and Indian Ocean Dipole

Fig. 7a shows the index of IOD mode, which is defined by anomalous SST difference between the western and southeastern equatorial Indian Oceans. The positive (negative) index refers to the positive (negative) IOD event.

Related BoB circulation is determined by examining the monthly mean geostrophic velocity fields of April, July and October in 1994, 1997 and 2006 (Fig. 7b). Among these, 1997 was the strongest positive IOD year followed by 1994 and 2006 was a weak positive IOD year.

According to Vinayachandran et al., (1999b) the zonal wind anomalies during IOD events weaken and reverse the equatorial flow. The eastward spring equatorial jet was not visible in the velocity fields of April 1994 and 1997. The direct current estimates (Reppin et al., 1999) also showed the weakening of spring jet in 1994 and its eastward extended up to 80°E (Vinayachandran et al., 1999a). In July 1994, a strong westward flow had appeared near the equator with speeds of about 1 m/s westward up to 87°E form the west of Sumatra. This current was found to extend northward up to 2°N and was an indication of IOD event. However, the westward flow was weakened and limited to east of 88°E, and the fall jet (October) was not developed in 1994. Meanwhile, the westward flow was strongly developed in October 1997 with speeds of up to 1.2 m/s. This indicates that the IOD condition attained earlier in 1994 than in 1997. It was reported (Vinayachandran et al., 1999a) that the 1994 IOD event occurred two months earlier than the 1997 event.

Although the equatorial jet was absent in spring 1997, the fall was marked with a broad and strong westward flow between the equator and 3°N with speeds of above 1 m/s. This was the clear signal of the IOD event in the surface flow pattern. Compared to 1994 and 2006, the IOD expression was very strong in the surface circulation in 1997. In 2006, the eastward equatorial jet was visible in the western part between 80°E and 87°E in spring. But in fall, westward current in 2006 occupies east of 90°E and was weak compared to than in1997. The IOD signal was weak in 2006 and the pattern in SST anomaly in the Equatorial Indian Ocean has been identified (Vinayachandran et al., 2007) during October-December.

The variations of surface circulation during positive and negative IOD years were determined from monthly mean geostrophic velocity fields of October, November and December in 1996, 1997 and 1998 (Fig. 7c). Among these years, 1997 was the strongest positive IOD year, 1996 was a strong negative IOD year, and 1998 was a slightly weak negative IOD year. In October, the southward-flowing western boundary current and the eastward-flowing equatorial jet were prominent in negative IOD years (1996 and 1998) with speeds of up to 1 m/s. Meanwhile, distinctive flow pattern occurs in 1997, especially near the equator and at the western boundary. The flow near the equator was reversed towards the west. There was no organised flow at the western boundary instead, a number of mesoscale eddies occupy the western boundary with speeds of up to 0.7 m/s.

The western boundary current was further strengthened in November 1996 and 1998 and intense flow with speeds of up to 1.3 m/s occurs between 5°N and 20°N. On the other hand, in 1997 the westward flow near the equator also had been strengthened, especially in the eastern part. By December, as the IOD condition was weakened, the western boundary current was slightly weakened in negative IOD years (1996 and 1998) and the westward jet near the equatorial region was also weakened in the positive IOD year (1997), occurring only west of 85°E. Thus, the strong western boundary current and eastward equatorial jet prevails in negative IOD years. During positive IOD year, the equatorial jet flows opposite to the normal years and the western boundary region shows weak eddy-embedded flow pattern. A difference of 0.5 m/s in current speed is found between positive and negative IOD years at the western boundary.

The surface circulation in 1997 exhibited a strong westward flow in the equatorial region up to 3°N. Thus, during positive IOD years, surface circulation shows the outflow from the BoB to Arabian Sea along the equatorial region. In negative IOD year, Arabian Sea water was entering through near the equatorial region, reaches up to central BoB and finally recirculates to the Arabian Sea through the strong broad western boundary flow.

The surface circulation during positive and negative IOD years were compared with the neutral year using composite maps of geostrophic velocity fields for October, November and December (Fig. 7d). Composite maps are prepared using positive IOD years of (1994, 1997 and 2006), negative IOD years of (1996, 1998 and 2005) and the neutral years of (2000, 2001 and 2004). During neutral period, the western boundary current is southward with a maximum speed of 1 m/s between 5°N and 12°N. Broad eastward flow occurs near the equator with a speed of 0.5 m/s and is stronger at the eastern end. Compared with the neutral period, during positive IOD period, the western boundary current is weak (less than 0.6 m/s) and the direction of eastward-flowing equatorial flow is reversed (with speed of 0.6 m/s). During negative IOD period, the southward flowing western boundary current is broad and very strong with a maximum speed of 1.2 m/s between 5°N and

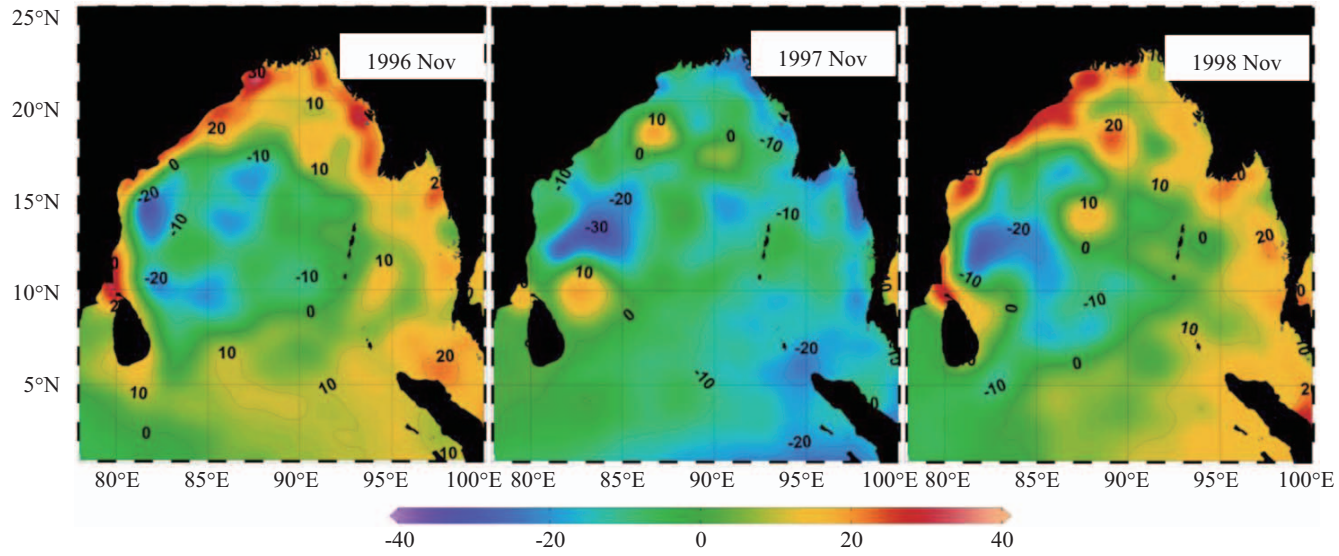

Fig. 8. Monthly mean sea level anomaly fields of November in 1996 (left panel), 1997 (middle) and 1998 (right).

20°N. The flow near the equator is eastward with a maximum speed of 0.6 m/s.

The monthly mean sea level anomaly fields of November 1996, 1997 and 1998 (Fig. 8) show high positive anomalies in the northern part of the BoB in negative IOD years of 1996 and 1998 and this positive anomaly propagated southward along the western boundary.

Interestingly, the strong zonal gradient in sea level anomaly was visible in the western boundary region, where strong currents exist. In contrary, in positive IOD year of 1997, the sea level anomaly was decreased and the zonal gradient also disappeared in the western boundary region. This is due to the propagation of negative anomalies from the southeastern BoB and the anomalies were radiated to the west through the Rossby waves. Thus, the sea level anomaly field is consistent with weakening of the western boundary current during positive IOD event.

5. Eddy Kinetic Energy

The eddy kinetic energy (EKE) is derived from the zonal and meridional velocity anomalies (u' and v') as

$$\mathbf{EKE} = \tfrac{1}{2}\,(\mathbf{u'^2 + v'^2}) \qquad (6)$$

The distribution of EKE averaged over the period of 1993-2009 shows higher EKE near the equatorial region and in the western part of the BoB (Fig. 9). The central and eastern parts shows very low EKE values. Thus, EKE distribution implies that large current variability occurs in the western boundary and near the equatorial region. The seasonal mean EKE averaged for the whole basin (Fig. 10) varies between 0.025 and 0.05 m^2/s^2 during 1993-2009. Besides seasonal signals, interannual variability is also prominent. Minimum EKE variation was found during 2003-2005. Higher anomalies were visible during 1994-1995, 1997-1998 and 2005-2006, and persisted for almost nine months.

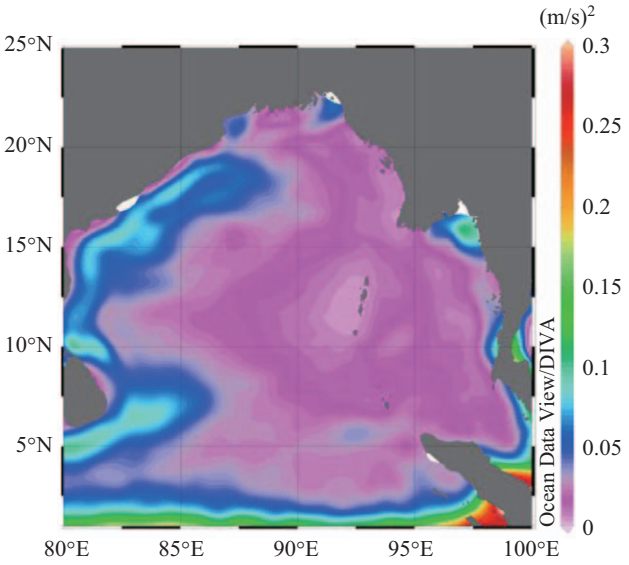

Fig. 9. Distribution of EKE averaged during 1993-2009.

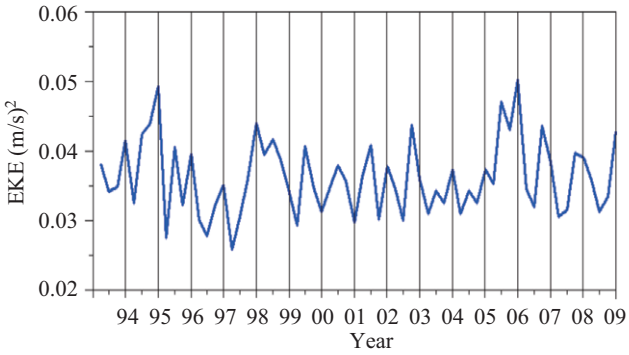

Fig. 10. Time series of seasonal mean of the basin-wide average EKE during 1993-2009.

Remarkably, these periods coincide with positive IOD/El

Niño events, and particularly the period of 1997-1998 (strong Dipole/El Niño) is marked with a longer persistence of high anomaly without much seasonal change than the other years. Hence, during strong IOD years, extended eddy activity was present. This is consistent with the flow characteristics obtained during positive IOD events, where the western boundary current is not continuous and instead it is embedded with number of mesoscale eddies.

IV. CONCLUSIONS

Combining the satellite altimetry and satellite-tracked surface drifter observations, the present study successfully brings out details of the surface circulation of the BoB and its mesoscale variability. The estimated velocity field is validated against in-situ observations and is consistent with correlation coefficient of above 0.7.

The major features in the mean flow field are the western boundary current (EICC), the weak westward NEC and significant eastward flows near the equator. The central BoB displays dull circulation. The EICC is the strongest current in the BoB and its mean speed reaches above 0.7 m/s. The Summer Monsoon Current and the equatorial jet are also prominent. Both EICC and NEC show strong seasonal variations. The eastward-flowing equatorial jet is identified both in spring and fall. Besides strong currents, strong mesoscale eddy activity is found in the western BoB.

The sea level anomaly shows unusual changes along the coastal regions during IOD/ElNiño events. In addition to the current reversal in the equatorial region, significant changes are seen in the western boundary flow pattern during IOD events. Both positive and negative IOD conditions immensely influence the western boundary flow pattern. During positive IOD event, the western boundary current is weak and embedded with mesoscale eddies, whereas a well-organised strong western boundary current prevails during negative IOD events. Higher EKE occurs near the equator and in the western boundary region. The annual variability of EKE illustrates high EKE during IOD/ El Niño years.

ACKNOWLEDGMENTS

The first author acknowledges financial support for the work from Fundamental Research Grant Scheme (FRGS) research grant Vote no. RJ1310000.7827.4F586, Ministry of Higher Education (MOHE). We used the altimeter data set produced by the Collect Localisation Satellites, the drifter data produced by the Atlantic Oceanographic and Meteorological Laboratory of the National Oceanic and Atmospheric Administration, and the wind data set produced and provided by the French Processing and Archiving Facility (CERSAT) at the French Research Institute for Exploration of the Sea. We used the Ocean Data View by R. Schlitzer (http://odv.awi.de, 2013), for preparing graphics. We appreciate the detailed and helpful comments of the anonymous reviewers of this manuscript.

REFERENCES

Annamalai, H. R., J. Potemra, S. P. Xie, P. Liu and B. Wang (2003). Coupled dynamics over the Indian Ocean: Spring initiation of the zonal mode. Deep Sea Research Part II 50, 2305-2330.

Aparna, S. G., J. P. McCreary, D. Shankar and P. N. Vinayachandran (2012). Signatures of Indian Ocean Dipole and El Niño-Southern Oscillation events in sea level variations in the Bay of Bengal. Journal of Geophysical Research 117, C10012.

Archiving, Validation and Interpretation of Satellite Oceanographic Data (AVISO), AVISO Handbook: Sea Level Anomaly Files (1997). 21st Edition. France, 24.

Babu, M. T., Y. V. B. Sarma, V. S. N. Murty and P. Vethamony (2003). On the circulation in the BoB during Northern spring inter-monsoon (March-April 1987). Deep Sea Research Part II 50, 855-865.

Benny, N. P. and K. Mizuno (2000). Annual cycle of steric heights in the Indian Ocean estimated from the thermal field. Deep Sea Research 47, 1351-1368.

Benny, N. P., D. Ambe, K. R. Mridula, S. Sahrum, K. M. Omar and M. Razali (2014). Mean and seasonal circulation of the south Indian Ocean estimated by combining satellite altimetry and surface drifter observations. Terrestrial Atmospheric and Oceanic Sciences 25, 91-106.

Chelton, D. B., M. G. Schlax, R. M. Samelson and R. A. de Szoeke (2007). Global observations of westward energy propagation in the ocean: Rossby waves or nonlinear eddies?. Geophysical Research Letter s 34, L15606.

Duing, W. (1970). The Monsoon Regime of the Currents in the Indian Ocean. East-West Center Press, Honolulu, 68.

Eigenheer, A. and D. Quadfasel (2000).Seasonal variability of the Bay of Bengal circulation inferred from TOPEX/Poseidon altimetry. Journal of Geophysical Research105, 3243-3252.

Halkides, D. J., W. Han and P. J. Webster (2006). Effects of the seasonal cycle on the development and termination of the Indian Ocean zonal dipole mode. Journal of Geophysical Research 111, C12017.

Horii, T., H. Hase, I. Ueki and Y. Masumoto (2008). Oceanic precondition and evolution of the 2006 Indian Ocean dipole. Geophysical Research Letter 35, L03607.

Jiang, X. and J. Li (2011). Influence of the annual cycle of sea surface temperature on the monsoon onset. Journal of Geophysical Research 116, D10105.

Li, T., Y. Zhang, C. P. Chang and B. Wang (2001).On the relationship between Indian Ocean sea surface temperature and Asian summer monsoon. Geophysical Research Letter 28, 2843-2846.

McCreary, J. P., W. Han, D. Shankar and S. R. Shetye (1996). Dynamics of the east Indian Coastal Current. 2. Numerical solutions. Journal of Geophysical Research 101(C6) 13,993-14,000.

Meyers, G., P. McIntosh, L. Pigot and M. Pook (2007). The years of El Niño, La Nina and interactions with the tropical Indian Ocean. Journal of Climate 20, 2872-2880.

Murty, V. S. N., Y. V. B. Sarma and D. P. Rao (1996). Variability of the oceanic boundary layer characteristics in the northern Bay of Bengal during MONTBLEX-90. Earth and Planetary Science Letters 105, 41-61.

Murty, V. S. N., Y. V. B. Sarma, D. P. Rao and C.S. Murty (1992). Water characteristics, mixing and circulation in the Bay of Bengal during southwest monsoon. Journal of Marine Research 50, 207-228.

Niiler, P. P. and D. Paduan (1995).Wind-driven motions in the northeast Pacific as measured by Lagrangian drifters. Journal of Physical Oceanography 25, 2819-2830.

Pant, V., M. S. Girishkumar, T. V. S. Udaya Bhaskar, M. Ravichandran, F. Papa and V. P. Thangaprakash (2015). Observed inter annual variability of near-surface salinity in the Bay of Bengal. Journal of Geophysical Research: Oceans, 120.

Paul, S., A. Chakraborty, P. C. Pandey, S. Basu, S. K. Satsangi and M. Ravi-

chandran (2009). Numerical simulation of Bay of Bengal circulation features from ocean general circulation model. Marine Geodesy 32, 1-18.

Pazan, S. E. and P. P. Niiler (2001). Recovery of near surface velocity from undrogued drifters. Journal of Atmospheric and Oceanic Technology 18, 476-479.

Pickard, G. L. and W. J. Emery (1982). Descriptive Physical Oceanography. 4th Edition. Pergamon Press, Oxford, 249.

Potemra, J. T., M. E. Luther and J. O'Brien (1991). The seasonal circulation of the upper ocean in the Bay of Bengal. Journal of Geophysical Research 96(C7), 12,667-12,683.

Ralph, A. E. and P. P. Niiler (1999).Wind-driven currents in the tropical Pacific. Journal of Physical Oceanography 29, 2121-2129.

Rao, R. R., M. S. Girish Kumar, M. Ravichandran, A. R. Rao, V. V. Gopalakrishna and P. Thadathil (2009). Inter annual variability of Kelvin wave propagation in the wave guides of the equatorial Indian Ocean, the coastal Bay of Bengal and the southeastern Arabian Sea during 1993-2006. Deep Sea Research Part I 57, 1-13.

Ratna Reddy, S., A. K. Easton, S. R. Clarke, A. NarendraNath and M. V. Rao (1995). Gyres off Somali coast and western boundary currents in the Bay of Bengal during the south-west monsoon. Int. Journal of Remote Sensing 16(9), 1679-1684.

Reppin, J., F. A. Schott, J. Fischer and D. Quadfasel (1999). Equatorial currents and transports in the upper central Indian Ocean. Journal of Geophysical Research 104, 15495-15514.

Saji, N. H., B. N. Goswami, P. N. Vinayachandran and T. Yamagata (1999). A dipole mode in the tropical Indian Ocean. Nature, 401, 360-363.

Sanilkumar, K. V., T. V. Kuruvilla, D. Jogendranath and R. R. Rao (1997). Observations of the western boundary current of the Bay of Bengal from a hydrographic survey during March 1993. Deep Sea Research 744, 135-145.

Schott, F. A. and J. P. McCreary (2001). The monsoon circulation of the Indian Ocean. Progress in Oceanography 51, 1-123.

Shankar, D., J. P. McCreary, W. Han and S. R. Shetye (1996). Dynamics of the East India Coastal Current 1. Analytic solutions forced by interior Ekman pumping and local alongshore winds. Journal of Geophysical Research 101.

Shankar, D., S. Shetye and P. Joseph (2007). Link between convection and meridional gradient of sea surface temperature in the Bay of Bengal. Journal of Earth System Science116, 385-406.

Shenoi, S. S. C., D. Shankar and S. R. Shetye (2002). Differences in heat budgets of the near-surface Arabian Sea and Bay of Bengal: Implications for the summer monsoon. Journal of Geophysical Research 107, 3052.

Shetye, S. R., A. D. Gouveia, D. Shankar, S. S. C. Shenoi, P. N. Vinayachandran, D. Sundar, G. S. Michael and G. Nampoothiri (1996). Hydrographyand circulation in the western BoB during the northeast monsoon. Journal of Geophysical Research 101, 14,011-14,025.

Shetye, S. R., A. D. Gouveia, S. S. C. Shenoi, D. Sundar, G. S. Michael and G. Nampoothiri (1993). The western boundary current of the seasonal subtropical gyre in the BoB. Journal of Geophysical Research 98, 945-954.

Stramma, L., J. Fischer and F. Schott (1996). The flow field off southwest India at 8°N during the southwest monsoon of August 1993. Journal of Marine Research 54, 55-72.

Tomczak, M. and S. Godfrey (1994). Regional Oceanography: An Introduction. Pergamon Press, New York.

Uchida, H. and S. Imawaki (2003). Eulerian mean surface velocity field derived by combining drifter and satellite altimeter data. Geophysical Research Letter 30(5), 1229.

Varkey, M., V. S. N. Murty and A. Suryanarayana (1996). Physical oceanography of the Bay of Bengal and Andaman Sea.Oceanography and Marine Biology (an annual Review) 34, 1-70.

Vinayachandran P. N., P. A. Francis and S. A. Rao, (2009). Indian ocean dipole: Processes and Impacts. In Current Trends in Science, Platinum Jubilee Special, Indian Academy of Sciences, 569 589.

Vinayachandran, P. N., S. Iizuka and T. Yamagata (2002). Indian Ocean dipole mode events in an ocean general circulation model. Deep Sea Research Part II, 49, 1573-1596.

Vinayachandran, P. N., J. Kurian and C. P. Neema (2007). Indian Ocean response to anomalous conditions in 2006. Geophys. Res. Lett. 34, L15602.

Vinayachandran, P. N., N. H. Saji and T. Yamagata (1999b). Response of the equatorial Indian Ocean to an anomalous wind event during 1994. Geophysical Research Letter 26, 1613-1615.

Vinayachandran, P. N., Y. Masumoto, T. Mikawa and T. Yamagata (1999a). Intrusion of the Southwest Monsoon Current into the Bay of Bengal. Journal of Geophysical Research 104, 11077-11085.

Webster, P. J., A. M. Moore, J. P. Loschnigg and R. R. Leben (1999). Coupled ocean-atmosphere dynamics in the Indian Ocean during 1997-98. Nature 401, 356-360.

Wyrtki, K (1973). An equatorial jet in the Indian Ocean. Science181, 262-264.

Wyrtki, K. (1971). Oceanographic Atlas of the International Indian Ocean Expedition. National Science Foundation, Washington D.C., 531.

Yamagata, T., S. K. Behara, S. A. Rao, Z .Gaun, K. Ashok and N. H. Saji (2002). The Indian Ocean dipole: A physical entity. CLIVAR Exchanges, 24 15-18, 20-22.